A comparison of the extended x-ray absorption fine structure of nanocrystalline ZrO_2 prepared by high-energy ball milling and other methods

2003 J. Phys.: Condens. Matter 15 431

(http://iopscience.iop.org/0953-8984/15/3/308)

INSTITUTE OF PHYSICS PUBLISHING JOURNAL OF PHYSICS: CONDENSED MATTER

J. Phys.: Condens. Matter **15** (2003) 431–440 PII: S0953-8984(03)52272-X

A comparison of the extended x-ray absorption fine structure of nanocrystalline ZrO_2 prepared by high-energy ball milling and other methods

Alan V Chadwick[1], **Marina J Pooley**[1,3], **K Erasmus Rammutla**[1], **Shelley L P Savin**[1] **and Aline Rougier**[2]

[1] Centre for Materials Research, School of Physical Sciences, University of Kent, Canterbury, Kent CT2 7NR, UK
[2] Laboratoire de Réactivité et Chimie des Solides, UMR 6007, Université Picardie Jules Verne, 33 rue St Leu, 80039 Amiens Cedex, France

E-mail: avc@ukc.ac.uk

Received 12 August 2002, in final form 11 December 2002
Published 13 January 2003
Online at stacks.iop.org/JPhysCM/15/431

Abstract

We report the results of an extended x-ray absorption fine structure (EXAFS) study of a sample of ZrO_2 prepared by high-energy ball milling. X-ray diffraction showed that the sample contained nanocrystals that were predominantly monoclinic with a particle size of 15 nm. The EXAFS for the sample was strongly attenuated in comparison to that for bulk monoclinic ZrO_2. This has been interpreted as the ball-milled sample containing a large level of disorder whose possible origins are discussed. In contrast, our previous EXAFS studies of nanocrystalline oxides prepared by sol–gel methods have shown that these samples contain well-ordered crystallites with grain boundaries similar to those in bulk materials. It is concluded that ball-milled samples are very different from oxide nanocrystals produced by other techniques.

1. Introduction

There is intense interest in nanocrystalline materials since their properties can be markedly different from the parent bulk solids [1–4]. Reasons for the interest in nanocrystalline ceramic oxides include the possibilities of producing superhard and superplastic ceramics and catalysts with enhanced activities. Clearly, the increased surface area to volume ratio afforded by preparing a catalyst in nanocrystalline form will increase activity, however, recent work on simple binary oxides [5] suggests that other factors, i.e. surface morphology and surface chemistry, are advantageously different for nanocrystals. In addition, nanocrystalline materials will dissolve higher concentrations of impurities than their bulk counterparts and

[3] Author to whom any correspondence should be addressed.

this offers further scope for tailoring new catalytic materials. A thorough understanding of the physics and chemistry of these new materials is reliant on a detailed characterization and, in particular, it is important to know the effect of the preparative route on the nature of the microstructure of the nanocrystal. Several methods have been developed to prepare nanocrystalline oxides including the calcination of hydroxides [6, 7], sol–gel syntheses [8–10], oxidation of nanocrystalline metals [11, 12], chemical vapour phase deposition [13, 14], radio-frequency sputtering [15, 16] and high-energy ball milling [17–20]. It is far from clear whether the different routes produce the same microstructure and the aim of this paper is to compare the microstructure of nanocrystalline zirconia produced by different routes.

We have used extended x-ray absorption fine structure (EXAFS) to study nanocrystalline zirconia. There is a long history of EXAFS measurements, a probe of local structure up to 5–10 Å [21], being used to determine the microstructure of nanocrystalline materials as the presence of disorder in a sample results in an attenuation of the amplitude of the oscillations. Early work on nanocrystalline metals reported strongly attenuated signals that were interpreted as evidence of highly disordered interfacial regions (see, for example, the study of nanocrystalline Cu [22]) and this view of the microstructure was assumed for all nanocrystalline materials. The interfacial region has even been termed 'gas-like'. However, more recent work has shown that the EXAFS signal is strongly dependent on sample preparation and the EXAFS protocol [23, 24]. The EXAFS of 12 nm nanocrystalline Pd produced by inert gas condensation and carefully selected for particle size homogeneity showed only a small attenuation of the signal [23]. This could be explained simply in terms of size effect with no evidence of high levels of disorder. Recent transmission EXAFS experiments for 13 nm nanocrystalline Cu showed no significant attenuation, leading to the conclusion that the interfaces were similar to normal grain boundaries found in bulk samples [24]. In contrast, the EXAFS of 8 nm nanocrystalline Fe produced by ball milling showed a strongly attenuated signal that was interpreted in terms of a large density of defects and ill-coordinated surface atoms in the material [25].

The history of EXAFS studies of nanocrystalline oxides is similar to that described above for metals, with papers both for and against the presence of highly disordered interfaces. However, there is now reliable EXAFS evidence for the interfaces being similar to normal grain boundaries in bulk samples. For the specific case of sol–gel-prepared tin oxide, SnO_2, see [26–29] and for zinc oxide, ZnO, see [30–32]. Reference [29] on 3 nm nanocrystals of SnO_2 shows that the nanocrystals have a similar level of static and dynamic disorder to that found in bulk material. Recent EXAFS studies of nanocrystalline zirconia, ZrO_2 [33–35], yttrium-stabilized cubic ZrO_2 (YSZ) [33–35] and CeO_2 [34, 35] prepared by polymer-spin coating (a variation of the sol–gel procedure) also reveal low levels of static and dynamic disorder. This seems to be a common feature of the sol–gel-synthesized nanocrystalline oxides [36].

High-energy ball milling has many potential advantages as a route to preparing nanocrystalline samples [20]. It can be applied to a wide range of material types, provides control over the particle size, produces large quantities of sample in short times and the equipment is relatively simple and inexpensive. Although detailed examinations of the microstructure on ball-milled samples are sparse, the very recent and thorough study of corundum, Al_2O_3, was particularly revealing [37]. In this work Al_2O_3 was ball milled down to an average particle size of 13 nm and examined by x-ray diffraction (XRD), transmission electron microscopy (TEM), ^{27}Al magic angle spinning nuclear magnetic resonance (MAS-NMR) and electron paramagnetic resonance (EPR) of the Fe^{3+} trace impurity. All the techniques revealed a significant fraction of amorphous material in the sample, around 80% from MAS-NMR and 50% from XRD, and the authors suggested the sample consisted of nanocrystalline grains embedded in amorphous grain boundaries. This is clearly very different

from the microstructure of sol–gel-prepared nanocrystalline oxides revealed by EXAFS [36] and was a stimulus for the work reported here.

Zirconia is an exceptionally important technological ceramic with a variety of applications, including use as a tough engineering material [38], a highly durable catalyst [39] and catalyst support [40] and as an oxygen conducting solid electrolyte membrane [41]. The normal phase of pure ZrO_2 at room temperature is monoclinic which converts at elevated temperatures to a tetragonal and then a cubic, fluorite-structured phase. The tetragonal phase can be stabilized at room temperature by the addition of small amounts ($\lesssim$16 mol%) of aliovalent cation impurities, such as Ca^{2+}, Mg^{2+} or Y^{3+}. Higher concentrations of these dopants will stabilize the cubic form at room temperature and it is this material, particularly the yttrium-stabilized cubic zirconia, YSZ, which is used as a solid electrolyte [41]. The tetragonal phase is also stabilized in small crystallites ($\lesssim$30 nm) of pure ZrO_2 [42]. In fact the common synthetic route to zirconia, the calcination of the hydroxide, produced by sol–gel procedures can be controlled via the annealing temperature and time, to control the particle size and phase. For example, heating for one hour at 500 °C will produce tetragonal crystallites with an average size of 10 nm, as measured from XRD [43]. However, the structural changes in the conversion from the hydroxide are complex [7, 44] and very recent work combining EXAFS and NMR measurements have emphasized the multiphase nature of ZrO_2 produced by calcination at low temperature [45]. Calcination temperatures in excess of 700 °C are necessary to remove traces of hydroxide and amorphous material from the sample. As a result, the final material has relatively large crystallites, average size $\sim$25 nm, and is a mixture of tetragonal and monoclinic phases.

There have been extensive EXAFS studies of ZrO_2, either pure or containing yttria stabilizer, to probe the local structure in bulk material [46] and nanocrystalline samples produced by calcining the hydroxide [7, 33–36, 44, 47–49], mechanical attrition of bulk ZrO_2 [17] or oxidation of the nanocrystalline metal [50, 51] and an unspecified chemical method [52]. We emphasize that the preparation route strongly affects the results and can lead to erroneous conclusions on the nature of the nanocrystals. It has been stated that the EXAFS results provide evidence of disordered surfaces in ZrO_2 nanocrystals prepared by hydroxide calcination as a consequence of the large fraction of atoms in the crystallite surface [48, 49]. These statements are incorrect as they ignore the presence of unreacted hydroxide in the sample [45] and the EXAFS of carefully prepared samples shows no evidence of disorder even in 6 nm nanocrystals [33–36]. The EXAFS of ball-milled ZrO_2 indicated the presence of amorphous material in the sample [17], however, that work provided only a qualitative analysis of the data and was performed before extensive studies were available for nanocrystalline ZrO_2 obtained from other preparation routes. In contrast, we will present below a detailed analysis of the EXAFS of ball-milled ZrO_2 and compare it with data for sol–gel-prepared samples collected and analysed by the same procedures by our group.

2. Experimental details

2.1. Materials

ZrO_2 powder (Prolabo, 99% purity) was ground using a Spex 8000 mixer mill, which generates essentially impact/shock interactions. Several samples were prepared but only the one with the smallest particle size was studied in depth. 1 g of powder was placed in a 50 ml stainless steel container together with five stainless steel balls (one of 14 mm, two of 8 mm and two of 6 mm diameter), leading to a ball/powder weight ratio of 26. Milling lasted for 60 min.

2.2. XRD

X-ray powder diffraction patterns of the samples were collected on a conventional laboratory diffractometer, a Phillips PW1720 instrument, using a Cu Kα tube operating at 35 kV and 20 mA. Particle sizes, S, were determined from the Scherrer equation [53], i.e.

$$S = \frac{K\lambda}{\beta \cos\theta}$$

where K is a constant (0.89), β is the full-width-at-half-maximum height of a diffraction peak at angle θ and λ is the x-ray wavelength.

2.3. EXAFS

Measurements were made on station 9.3 at the CLRC Daresbury synchrotron radiation source. The synchrotron has an electron energy of 2 GeV and the average current during the measurements was 150 mA. Station 9.3 is equipped with a high-stability, double Si(220) crystal monochromator that can be offset from the Bragg angle to reject harmonic contaminants from the monochromatic beam. In the present work the harmonic rejection was set at 50%. Zr K edge EXAFS spectra for the powdered materials were collected at room temperature in conventional transmission mode using gas-filled ion chamber detectors. The samples were prepared by thoroughly mixing the ground material with fumed silica or powdered polythene diluents and pressed into pellets in a 13 mm IR press. Spectra were typically collected to $k = 18$ Å^{-1} and several scans were taken to improve the signal-to-noise ratio. For these measurements, the amount of sample in the pellet was adjusted to give an adsorption of about $\mu d = 1$.

The data were processed in the conventional manner using the Daresbury suite of EXAFS programmes; EXCALIB, EXBACK (or EXBROOK) and EXCURV98 [54]. Phase shifts were derived from *ab initio* calculations within EXCURV98. This code also includes routines to treat multiple scattering effects in highly symmetric structures and these were employed in the current work. For each spectrum a theoretical fit was obtained by adding shells of atoms around the central excited atom and least-squares iterating the radial distances, RD, and the Debye–Waller type factors, $A(=2\sigma^2)$. This latter factor will contain contributions from both thermal disorder and static variations in RD. In some cases the co-ordination number (CN), was also iterated. The quality of the fit is measured by an R-factor [54] and the errors in RD are $\sim\pm 0.02$ Å and $\sim\pm 20\%$ in A and CN.

3. Results and discussion

The XRD pattern for the ball-milled sample is shown in figure 1 along with the patterns for monoclinic and tetragonal ZrO_2. The ball-milled sample is predominantly in the monoclinic phase and the particle size calculated by applying the Scherrer equation to the peak at 28.2° (the $\bar{1}01$ reflection) yields an average particle size of 15 nm. There is a shoulder on the peak at 31.5° (the 111 reflection) centred at about 30°, which corresponds to the 101 reflection of the tetragonal phase. From the peak areas we estimate that the amount of tetragonal phase in the sample is at most 10%, which should not present a major problem in analysing the EXAFS results in terms of the ball-milled material in the monoclinic phase.

The Zr K-edge EXAFS of the monoclinic ZrO_2 powder prior to ball milling is shown in figure 2. The fitting of the spectrum was performed using an initial structural model based on a simplified picture of the crystallographic data [33, 46] for the first four co-ordination shells. In the least-squares fitting, the CNs were held constant and radial distances and the

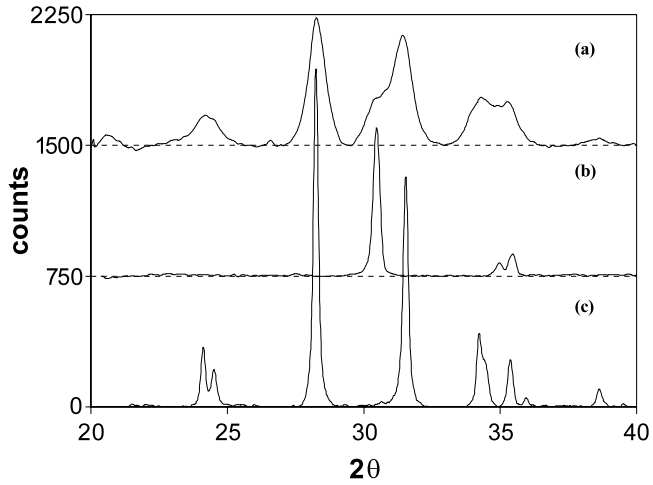

Figure 1. The XRD patterns for zirconia powders: (a) the ball-milled sample with 15 nm particle size, (b) tetragonal ZrO_2, (c) monoclinic ZrO_2.

Debye–Waller factors were allowed to float. The best-fit parameters are listed in table 1 along with previous EXAFS data for ZrO_2. It can be seen that the present parameters are in excellent agreement (within the expected experimental errors of ± 0.02 Å for the radial distances and $\pm 20\%$ for the Debye–Waller factors) with our previous study of monoclinic bulk ZrO_2 [33, 35], which provides a necessary validation of the current set of experiments. It is normal for the Debye–Waller factors to increase with increasing radial distance and therefore the large value for the Zr–O correlation (0.028 $Å^2$) compared to those for the Zr–Zr correlations is at first sight disconcerting. However, the crystallographic data for monoclinic ZrO_2 show that the Zr–O shell is complex with 7O atoms at seven different distances ranging from 2.051 to 2.285 Å. Following previous studies [33, 46], we have used a simplified model for this shell and the large Debye–Waller factor is due to the dispersion in the radial distances.

The Zr K-edge EXAFS of the ball-milled sample is shown in figure 3. A visual inspection of the plot shows that it is basically similar to that for the monoclinic bulk sample except for an attenuation of the EXAFS at large k and a marked reduction in the second (i.e. a factor of two) and higher peaks, the Zr–Zr correlations, in the Fourier transform centred at $\sim$3.5 Å. The spectrum was fitted using the same starting model for the bulk monoclinic sample (i.e. four co-ordination shells) and again the CNs were held constant and the radial distances and Debye–Waller factors were allowed to float. The best-fit parameters are listed in table 1. The radial distance and the Debye–Waller factor for the first shell, the Zr–O correlation, are virtually identical to those for the bulk material. In contrast, although the radial distances for the Zr–Zr correlations are very similar to those for the bulk material, the Debye–Waller factors are markedly increased, by nearly a factor of two, as expected from the reduction in peak size. Other approaches were taken to the fitting, i.e. allowing the CNs to float, and equally good fits were obtained to those shown in table 1. In these cases, the reduction in the magnitude of the Zr–Zr correlations was partly taken up by a reduction in the CNs, however, the radial distances remained essentially the same as for the bulk monoclinic sample. It should be noted that a particle size of 15 nm would have an insignificant effect on the CNs of the Zr–Zr shells [36].

The strong attenuation of the EXAFS of the ball-milled sample is clearly indicative of a high level of disorder in the sample. There are a number of possible origins for the disorder which EXAFS measurement alone will not be able to discriminate. One possibility is the

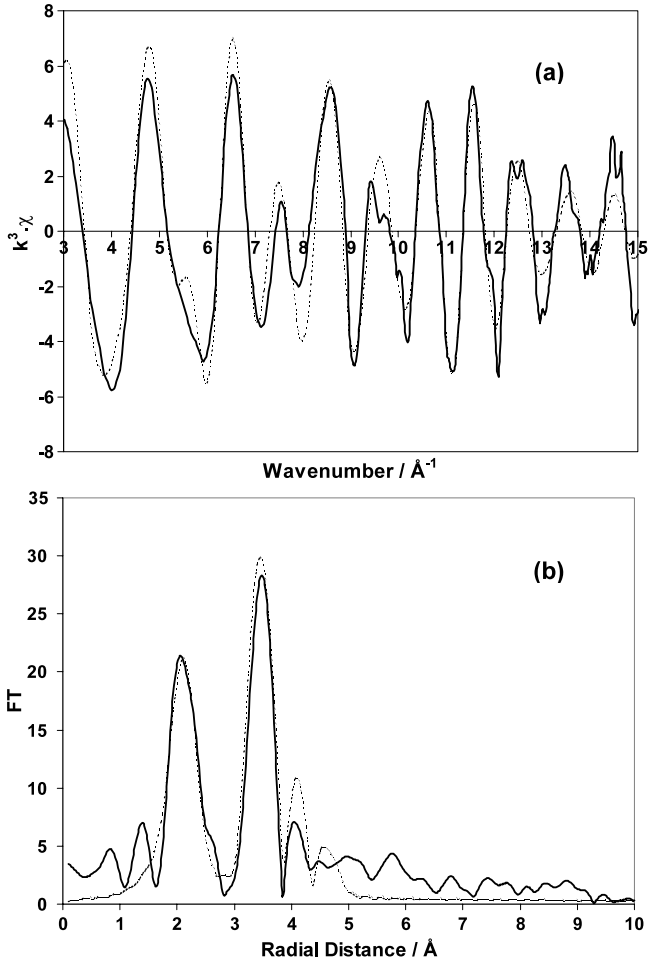

Figure 2. EXAFS spectra (k^3-weighted) and corresponding Fourier transforms for bulk monoclinic ZrO_2 powder; (a) and the corresponding Fourier transform (b) corrected with the phase shift of the first shell. The experimental data are shown by the solid curves and the best fit is the dotted curves.

presence of a large number of defects and ill-coordinated surface atoms in the crystallites, the model used to interpret the EXAFS of ball-milled Fe [25]. These could be either point defects or dislocations. Another possibility is that the interfaces between the crystallites are highly disordered, the situation discussed in the introduction for the early work on nanocrystalline metals. However, there is good evidence from TEM that ball-milled ZrO_2 [17] and Al_2O_3 [37] contain considerable portions of amorphous material. Therefore, for the purpose of comparison with the recent data for Al_2O_3 it is worth pursuing a model that assumes that the EXAFS shown in figure 3 is for a two-phase sample, containing nanocrystals of monoclinic ZrO_2 and amorphous ZrO_2, and then make a semi-quantitative analysis of the composition. An upper limit to the fraction of crystalline material in the sample can be obtained by assuming that the amorphous material is completely disordered beyond the first Zr–O shell, i.e. there are no peaks beyond the first peak in the Fourier transform of the amorphous material. On this basis the second peak in the Fourier transform of the ball-milled sample at 3.45 Å is due only to Zr atoms in the crystalline region of the sample. The ratio of the area of this second peak for the

Table 1. EXAFS results for nanocrystalline zirconia powders and precursors (errors on the parameters are quoted in the text).

			Zr K edge EXAFS				
Composition	Grain size	Phase	Atom	CN	RD (Å)	A ($Å^2$)	Comment/Reference
Zirconium hydroxide	Bulk	Amorphous	O	7	2.13	0.018	Room temperature [33]
			Zr	4	3.37	0.028	
Zirconium hydroxide	Bulk	Amorphous	O	2.0 ± 0.5	2.08	0.01	Room temperature [7]
			O (or OH/H_2O)	5 ± 0.5	2.16	0.022	
			Zr	1.7 ± 1.0	3.27	0.023	
			Zr	2.0 ± 1.0	3.41	0.023	
ZrO_2	Bulk	Monoclinic	O	7	2.15	0.020	Room temperature [33]
			Zr	7	3.46	0.015	
			Zr	4	4.03	0.017	
			Zr	1	4.55	0.002	
ZrO_2	Bulk	Monoclinic	O	7	2.14	0.026	Room temperature This work
			Zr	7	3.45	0.016	
			Zr	4	3.98	0.019	
			Zr	1	4.54	0.007	
ZrO_2 ball milled	15 nm	Monoclinic	O	7	2.13	0.028	Room temperature This work
			Zr	7	3.45	0.027	
			Zr	4	4.00	0.033	
			Zr	1	4.54	0.015	
YSZ	Bulk	Cubic	O	7	2.31	0.018	Room temperature [33]
			Zr(Y)	12	3.61	0.020	
YSZ film	6 nm	Cubic	O	7	2.33	0.018	Room temperature [33]
			Zr(Y)	12	3.63	0.016	

ball-milled and the bulk sample is therefore the fraction of crystalline material in the ball-milled sample. This analysis yields 60% amorphous material in the ball-milled sample. This will be an underestimate as the amorphous material would be expected to show some local structure beyond the first co-ordination shell and there would be some contribution to the second peak in the Fourier transform. Although we would not try to pursue this model too far, we believe it is noteworthy that an estimate of 60% is in the range of 50–80% reported for ball-milled Al_2O_3.

An attenuation of the EXAFS of ball-milled ZrO_2 has been noted by previous workers [17] and attributed to amorphous material in the sample. However, it was not treated by any detailed analysis; only the Zr–O correlation was analysed and no estimate was made of the phase composition of the sample. In addition, it was assumed by comparison with the earlier EXAFS of ZrO_2 nanocrystals prepared from the hydroxide [49] that an attenuation of the EXAFS was a common feature of all nanocrystalline samples. This is now known to be incorrect and that carefully prepared samples of nanocrystalline ZrO_2, even at a particle size of 6 nm show no perceptible attenuation [33–36]. An illustration of this can be seen in the parameters listed for bulk and 6 nm YSZ in table 1.

4. Conclusions

The experiments reported here show that the EXAFS of ball-milled ZrO_2 is strongly attenuated compared to that for the bulk material. This is clear evidence that the ball-milled sample

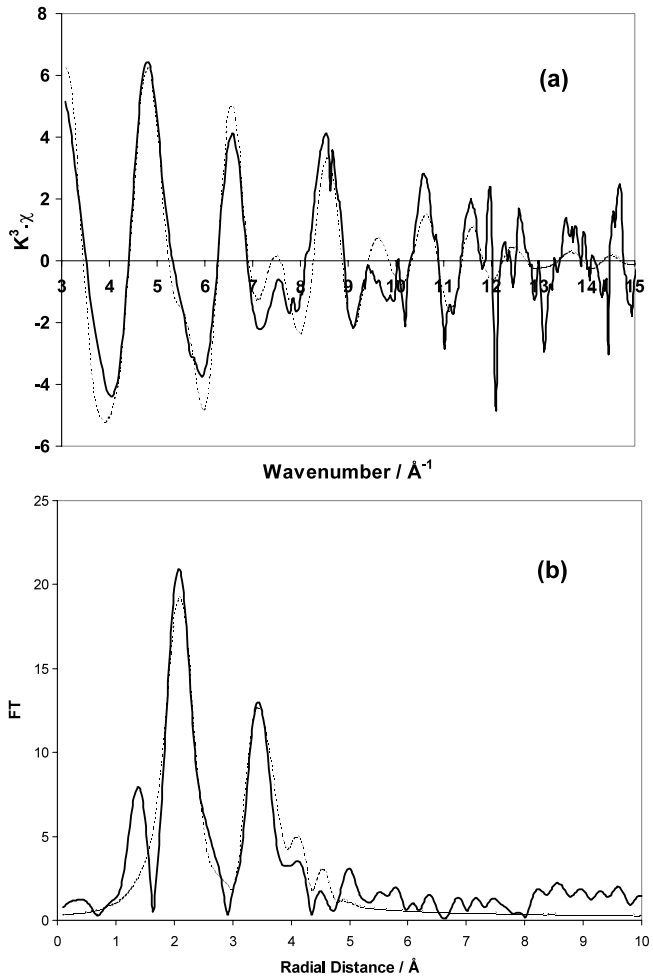

Figure 3. EXAFS spectra (k^3-weighted) and corresponding Fourier transforms for ball-milled ZrO_2 powder (15 nm) (a) and the corresponding Fourier transform (b) corrected with the phase shift of the first shell. The experimental data are shown by the solid curves and the best fit is the dotted curves.

contains a high level of disorder. On the basis of the EXAFS experiments alone it is not possible to identify the exact nature of the disorder. It is worth noting that applying the model recently developed for ball-milled Al_2O_3, in which the nanocrystals are embedded in an amorphous matrix [37], is consistent with the present results. It is a matter of opinion as to whether this model is any different to one in which the nanocrystallites are separated by disordered interfaces. In either case, detailed analysis of the EXAFS would require a two-phase model, i.e. Zr atoms in two different types of local environment.

The presence of disorder is a result of the ball-milling method of preparation and is not a general feature of nanocrystalline materials. We have shown that nanocrystalline films of ZrO_2 [34, 35] and YSZ [33, 35] prepared by polymer spin coating show no attenuation of the EXAFS even at particle sizes of 6 nm. Similar results for other nanocrystalline oxides prepared by the sol–gel technique show that the crystallites are well-ordered and that the interfaces between crystallites are like grain boundaries in normal bulk samples [36].

We conclude that nanocrystalline oxide samples prepared by ball milling should be considered separately from samples prepared by other techniques. The presence of disorder, which is not present in samples prepared by other methods, could well be the origin of some of the unusual properties reported for ball-milled samples. A particularly important case is that of anomalously high diffusion coefficients [20, 55]. For example, anomalously fast Li^+ ion diffusion has been reported from NMR studies of ball-milled $LiNbO_3$ with a particle size of 22 nm. Preliminary studies of the EXAFS of ball-milled $LiNbO_3$ show an attenuation of the spectrum similar to that reported here [56]. It is therefore important to ascertain whether fast diffusion in ball-milled samples is simply due to the inherent disorder in these particular samples or whether it is an intrinsic property of nanocrystalline materials. Hence, parallel diffusion studies of ball-milled and sol–gel samples are needed to resolve this important issue.

Acknowledgments

We thank Hilger Crystals and the EPSRC for the award of a CASE studentship to MJP. The authors are grateful to the staff of the Daresbury SRS, particularly Drs Dent, Harvey and Mosselmanns, for assistance with the experiments.

References

[1] Gleiter H 1992 *Adv. Mater.* **4** 474
[2] Seigel R W and Fougere G E 1995 *Nanostruct. Mater.* **6** 205
[3] Gleiter H 2000 *Acta Mater.* **48** 1
[4] Knauth P 2002 *J. Solid State Electrochem.* **6** 165
[5] Stark J V, Park D G, Lagadic I and Klabunde K J 1996 *Chem. Mater.* **8** 1904
[6] Bokhimi X, Morales A, Portilla M and Gracia-Ruiz A 1999 *Nanostruct. Mater.* **12** 589
[7] Turillas X, Barnes P, Dent A J, Jones S L and Norman C J 1993 *J. Mater. Chem.* **3** 583
[8] Schneider M and Baiker A 1995 *Catal. Rev. Sci. Eng.* **37** 515
[9] Pascual R, Sayer M, Kumar C V R V and Zou L 1991 *J. Appl. Phys.* **70** 2348
[10] Bokhimi X, Morales A, Lopez T and Gomez 1995 *J. Solid State Chem.* **115** 411
[11] Hahn H, Eastman J A and Seigel R W 1998 *Ceramic Trans. 1b. Ceramic Powder Science* 1115
[12] Hahn H 1997 *Nanostruct. Mater.* **9** 3
[13] Kim E-T and Yoon S-G 1993 *Thin Solid Films* **7** 227
[14] Barreca D, Battiston G A, Caccavalec F, di Noto V, Gerbasi R, Gregori A, Rizzi G A, Tiziani A and Tondello E 1999 *J. Physique* IV **9** 539
[15] Luo W G, Ding A L and Li H 1995 *Integr. Ferroelectr.* **9** 75
[16] Manovsky A A, Liu J P, Gelders H J, Harrison B J, Ellermeyer H and Huang Y K 1996 *Mater. Sci. Eng.* A **217** 227
[17] Michel D, Gaffet E and Berthet P 1995 *Nanostruct. Mater.* **6** 667
Michel D, Mazerolles L, Berthet P and Gaffet E 1995 *Eur. J. Solid State Inorg. Chem.* **32** 673
[18] Tkacova K, Sepalak V, Stevulova N and Boldyrev V V 1996 *J. Solid State Chem.* **123** 100
[19] Shen T D, Koch C C, McCormick T L, Nemanich R J, Huang J Y and Huang J G 1995 *J. Mater. Res.* **10** 139
[20] Indris S, Bork D and Heitjans P 2000 *J. Mater. Synth. Process.* **8** 245
[21] Koningsberger D C and Prins R 1988 *X-Ray Absorption. Principles, Applications, Techniques of EXAFS, SEXAFS and XANES* (New York: Wiley)
[22] Haubold T, Birringer R, Lengeler B and Gleiter H 1989 *Phys. Lett.* A **135** 461
[23] de Panfilis S, d'Acapito F, Haas V, Konrad H, Weissmüller J and Boscherini F 1995 *Phys. Lett.* A **207** 397
[24] Stern E A, Siegel R W, Newville M, Sanders P G and Haskel D 1995 *Phys. Rev. Lett.* **75** 3874
[25] Di Cicco A, Berrettoni M, Stizza S, Bonetti E and Cocco G 1994 *Phys. Rev.* B **50** 12386
[26] Briois V, Santilli C V, Pulcinelli S H and Brito G E S 1995 *J. Non-Cryst. Solids* **191** 17
[27] Brito G E S, Ribeiro S J L, Briois V, Dexpert-Ghys J, Santilli C V and Puncinelli S H 1997 *J. Sol–Gel Sci. Technol.* **8** 261
[28] Brito G E S, Briois V, Puncinelli S H and Santilli C V 1997 *J. Sol–Gel Sci. Technol.* **8** 269
[29] Davis S R, Chadwick A V and Wright J D 1997 *J. Phys. Chem.* B **101** 9901

[30] Chadwick A V, Russell N V, Whitham A R and Wilson A 1994 *Sensors Actuators* B **18** 99
[31] Russell N V, Chadwick A V and Wilson A 1995 *Nucl. Instrum. Methods* B **97** 575
[32] Chadwick A V, Harsch A, Russell N V, Tse K F, Whitham A R and Wilson A 1995 *Radiat. Eff. Defects Solids* **137** 1277
[33] Rush G E, Chadwick A V, Kosacki I and Anderson H U 2000 *J. Phys. Chem.* B **104** 9597
[34] Rush G E, Chadwick A V, Kosacki I and Anderson H U 2001 *Radiat. Eff. Latt. Defects Solids* **156** 117
[35] Rush G E 2001 *PhD Thesis* University of Kent
[36] Chadwick A V and Rush G E 2001 *Nanocrystalline Metals and Oxides: Selected Properties and Applications* ed P Knauth and J Schoonman (Boston, MA: Kluwer)
[37] Scholz G, Stösser R, Klein J, Silly G, Buzaré J Y, Laligant Y and Ziemer B 2002 *J. Phys.: Condens. Matter* **14** 2101
[38] Srinivasan R and Davis B H 1997 *Materials Synthesis and Characterization (Am. Ceram. Soc. Symp. (San Diego, CA, March 1994))* ed D L Perry (Westerville, OH: American Ceramic Society) ch 9
[39] Yamaguchi T 1994 *Catal. Today* **20** 199
[40] Gomez R, Lopez T, Ferrat G, Dominguez J M and Schiffer I 1992 *Chem. Lett.* 1941
[41] Kilner J, Benson S, Lane J and Waller D 1997 *Chem. Ind.* **22** 907
[42] Garvie R C 1978 *J. Phys. Chem.* **82** 218
[43] Liu H, Feng L, Zhang X and Xue Q 1995 *J. Phys. Chem.* **99** 332
[44] Turillas X, Barnes P, Gascoigne D, Turner J Z, Jones S L, Norman C J, Pygall C F and Dent A J 1995 *Radiat. Phys. Chem.* **45** 491
[45] Chadwick A V, Mountjoy G, Nield V M, Poplett I J F, Smith M E, Strange J H and Tucker M G 2001 *Chem. Mater.* **13** 1219
[46] Li P, Chen I-W and Penner-Hahn J E 1993 *Phys. Rev.* B **48** 10063
Li P, Chen I-W and Penner-Hahn J E 1993 *Phys. Rev.* B **48** 10074
Li P, Chen I-W and Penner-Hahn J E 1993 *Phys. Rev.* B **48** 10082
[47] Brook H C, Chadwick A V, Kennedy K M, Morgante N, Rafeletos G, Tomba A and Roberts M A 1997 *Mater. Sci. Forum* **239–241** 687
[48] Wang Y R, Lu K Q, Wang D H, Wu Z H and Fang Z Z 1994 *J. Phys.: Condens. Matter* **6** 633
[49] Qi Z, Shi C, Wei Y, Wang Z, Liu T, Hu T, Zhao Z and Li F 2001 *J. Phys.: Condens. Matter* **13** 11503
[50] Nitsche R, Winterer M, Croft M and Hahn H 1995 *Nucl. Instrum. Methods* B **97** 127
[51] Winterer M, Nitsche R and Hahn H 1997 *Nanostruct. Mater.* **9** 397
[52] Deng H, Qiu H and Shi G 1995 *Physica* B **208/209** 591
[53] Klug H P and Alexander L E 1974 *X-Ray Diffraction Procedures* (New York: Wiley)
[54] Binsted N, Campbell J W, Gurman S J and Stephenson P C 1992 *SERC Daresbury Program Library* Daresbury Laboratory, Warrington, Cheshire WA4 4AD, UK
Binsted N 1998 *EXCURV98: CCLRC Daresbury Laboratory Computer Program*
[55] Bork D and Heitjans P 1998 *J. Phys. Chem.* B **102** 7303
[56] Pooley M J and Chadwick A V 2002 *Radiat. Eff. Latt. Defects Solids* at press